A First Assessment of IceBridge Snow and Ice Thickness Data Over Arctic Sea Ice

Sinéad Louise Farrell, Nathan Kurtz, Laurence N. Connor, Bruce C. Elder, Carlton Leuschen, *Member, IEEE*, Thorsten Markus, *Member, IEEE*, David C. McAdoo, Ben Panzer, Jacqueline Richter-Menge, and John G. Sonntag

***Abstract*—We present a first assessment of airborne laser and radar altimeter data over snow-covered sea ice, gathered during the National Aeronautics and Space Administration Operation IceBridge Mission. We describe a new technique designed to process radar echograms from the University of Kansas snow radar to estimate snow depth. We combine IceBridge laser altimetry with radar-derived snow depths to determine sea ice thickness. Results are validated through comparison with direct measurements of snow and ice thickness collected *in situ* at the Danish GreenArc 2009 sea ice camp located on fast ice north of Greenland. The IceBridge instrument suite provides accurate measurements of snow and ice thickness, particularly over level ice. Mean IceBridge snow and ice thickness agree with *in situ* measurements to within $\sim$0.01 and $\sim$0.05 m, respectively, while modal snow and ice thickness estimates agree to within 0.02 and 0.10 m, respectively. IceBridge snow depths were correlated with *in situ* measurements ($R = 0.7$, for an averaging length of 55 m). The uncertainty associated with the derived IceBridge sea ice thickness estimates is 0.40 m. The results demonstrate the retrieval of both first-year and multiyear ice thickness from IceBridge data. The airborne data were however compromised in heavily ridged ice where snow depth, and hence ice thickness, could not be measured. Techniques developed as part of this study will be used for routine processing of IceBridge retrievals over Arctic sea ice. The limitations of the GreenArc study are discussed, and recommendations for future validation of airborne measurements via field activities are provided.**

***Index Terms*—Altimetry, geophysical measurement techniques, remote sensing, sea ice, snow.**

Manuscript received March 28, 2011; revised July 19, 2011 and August 29, 2011; accepted September 18, 2011. Date of publication November 15, 2011; date of current version May 16, 2012. This work was supported by NOAA, and the NASA Cryospheric Sciences Program. The views, opinions, and findings contained in this report are those of the authors and should not be construed as an official National Oceanic and Atmospheric Administration or US Government position, policy, or decision.

S. L. Farrell is with the Earth System Science Interdisciplinary Center, University of Maryland, College Park, MD 20740 USA (e-mail: sineadf@umd.edu).

N. Kurtz was with the NASA—University of Maryland Baltimore County Joint Center for Earth Systems Technology, Baltimore, MD 21250 USA and also with the Hydrospheric and Biospheric Sciences Laboratory, NASA Goddard Space Flight Center, Greenbelt, MD 20771 USA. He is now with the Goddard Earth Sciences Technology and Research (GESTAR) Program, Morgan State University, Baltimore, MD 21251 USA (e-mail: nathan.t.kurtz@nasa.gov).

L. N. Connor and D. C. McAdoo are with the Laboratory for Satellite Altimetry, Satellite Oceanography and Climatology Division, National Oceanic and Atmospheric Administration, Silver Spring, MD 20910 USA (e-mail: laurence.connor@noaa.gov; dave.mcadoo@noaa.gov).

B. C. Elder and J. Richter-Menge are with the Cold Regions Research and Engineering Laboratory, U.S. Army Corps of Engineers, Hanover, NH 03755 USA (e-mail: Bruce.C. Elder@usace.army.mil; Jacqueline.A.Richter-Menge@usace.army.mil).

C. Leuschen and B. Panzer are with the Center for Remote Sensing of Ice Sheets, University of Kansas, Lawrence, KS 66045 USA (e-mail: leuschen@cresis.ku.edu; bpanzer@ku.edu).

T. Markus is with the Hydrospheric and Biospheric Sciences Laboratory, NASA Goddard Space Flight Center, Greenbelt, MD 20771 USA (e-mail: thorsten.markus@nasa.gov).

J. G. Sonntag is with the URS Corporation, NASA Wallops Flight Facility, Wallops Island, VA 23337 USA (e-mail: john.g.sonntag@nasa.gov).

Color versions of one or more of the figures in this paper are available online at http://ieeexplore.ieee.org.

Digital Object Identifier 10.1109/TGRS.2011.2170843

I. Introduction

RECENT results from satellite laser and radar altimetry missions including ICESat and Envisat have revealed a dramatic decline in Arctic sea ice freeboard, thickness, and volume since 2003 [1]–[4], and a substantial loss of the multiyear (MY) ice pack. These satellite altimetry missions have provided us the opportunity to estimate basin-scale sea ice thickness, although the combined observation period is short and precludes a definitive determination of the long-term variability in sea ice thickness. New and future missions will establish whether current observations are indeed part of a long-term, negative trend in Arctic sea ice thickness; the European Space Agency launched CryoSat-2 in April 2010, and the National Aeronautics and Space Administration (NASA) ICESat-2 mission is planned for launch in 2016 [5]. In the interim, through a sustained collection of airborne remote sensing data over critical areas of the Arctic and Southern Ocean ice packs, NASA's Operation IceBridge mission will provide continuity between ICESat and ICESat-2.

Snow is an important component of the polar climate system. The low-density snow layer is a poor conductor of heat and acts as an insulator between the atmosphere and ocean, impacting the surface heat balance of the ice pack [6], as well as influencing the wintertime growth rate of sea ice [7]. Snow accumulation on sea ice floes affects the location, size, and depth of summer melt ponds, resulting in a dramatic change in albedo during the melt season [8, and references therein]. Moreover, it is critical for the retrieval of sea ice thickness from altimetric data; knowledge of snow loading combined with sea ice freeboard can be used to estimate ice thickness by assuming that sea ice floes are in local hydrostatic equilibrium [8]. For example, the Warren *et al.* [9] snow thickness climatology has been used to estimate snow loading for sea ice retrievals from satellite altimetry data including ERS-1 and -2 [10], Envisat [4] and ICESat [11]. An alternate approach using snow thickness models based on meteorological data has also been developed for use with satellite laser altimetry [1], [12].

Although the Warren *et al.* [9] climatology provides monthly mean snow depths, these monthly averages are based on

0196-2892/$26.00 © 2011 IEEE

TABLE I
DESCRIPTION OF DATA COLLECTED BY AIRBORNE AND GROUND-BASED INSTRUMENTS WITH AN ESTIMATE OF THE SINGLE SHOT ACCURACY, IF APPLICABLE. NOTE, DIMENSIONS FOR AIRBORNE MEASUREMENTS ARE BASED ON A FLIGHT ALTITUDE OF 490 m

Instrument	Measurement Approach	Platform	Parameter	Footprint (along-track) (m)	Footprint (cross-track) (m)	Sampling Frequncy (m)	Estimated Single Shot Accuracy (cm)
Airborne Topograhpic Mapper (ATM) Laser Altimeter	Scanning 532 nm laser profiler	Airborne/P-3	Surface Elevaton	~1	268	~5	5[α]
University of Kansas Snow Radar	2.5 -7 GHz FMCW radar	Airborne/P-3	Snow Depth	15	16	1	5[β]
CAMBOT digital camera	Nadir-looking digital photography	Airborne/P-3	Surface Characterisaton	~550	~370	~375	N/A
Geonics EM 31 MKII electormagnetic induction sounder	Electromagnetic ice thickness sounding	Ground	Sea Ice Thickness	~3	~3	5	10[γ]
Snow depth probe	Direct measurement of Snow depth	Ground	Snow Depth	N/A	N/A	5	1[δ]
Manual Drilling	Direct measurement of sea ice thickness and freeboard	Ground	Sea Ice Thickness; Sea Ice Freeboard	N/A	N/A	5	1[ζ]

Footnotes:
α Based on the standard deviation of ATM elevations over undeformed level ice adjacent to aircraft runway (see Table 2).
β From [17], based on the range resolution of the snow radar in the snow pack.
γ From [21], estimated for level sea ice.
δ J. Richter-Menge, personal communication
ζ J. Richter-Menge, personal communication

37 years (1954–1991) of measurements obtained at Soviet drifting stations on level MY ice. No contemporary, systematic, basin-scale observations of snow depth exist for Arctic Ocean sea ice. A routine monitoring of snow depth would therefore represent a major advancement in our observational capabilities of sea ice and would significantly improve the accuracy of large-scale sea ice thickness monitoring. Regional-scale mapping of snow depth on sea ice would also provide information on the mean precipitation rate in the Arctic [9] and its interannual variability.

Over the last decade, a number of studies have investigated the use of airborne or ground-based radar systems for the retrieval of snow thickness on sea ice. Radar penetration into the snow pack depends on the dielectric properties of the pack, which are influenced by snow density, temperature and wetness [13]. Data collected during the Laser Radar Altimetry (LaRA) field campaign in 2002 were used to investigate the feasibility of combining laser and radar altimeter measurements over snow-covered sea ice to calculate the snow depth [14], the results of which were consistent with the snow thickness climatology. Dedicated ultrawideband frequency-modulated continuous-wave (FMCW) radars operating over the frequency range from 2–8 GHz have been developed to obtain direct measurements of snow depth on sea ice. Data gathered by an FMCW snow radar deployed on ice using a sled were highly correlated (to 0.95) with *in situ* snow depth measurements [15], while correlation coefficients for a helicopter-borne radar were between 0.53 and 0.57 [16], showing the potential for FMCW radar observations of snow thickness. IceBridge provides the first routine monitoring of snow on sea ice using an airborne FMCW snow radar system developed by the University of Kansas [17]. Indeed, the IceBridge instrument suite for sea ice observation typically consists of the snow radar, the airborne topographic mapper (ATM) laser altimetry system [18], and a digital camera system to record sea ice morphology.

In spring 2009, the GreenArc campaign was conducted in the high Arctic on sea ice north of Greenland by a consortium of Danish institutions in collaboration with international partners (see http://ocean.dmi.dk/arctic/icecamp/index.php). The primary goal of this International Polar Year project was to assess the regional response of the sea ice environment to Arctic climate variability. During GreenArc 2009, an ice camp was established on fast ice near the northern coast of Greenland, and an *in situ* survey of the area was coordinated by the Cold Regions Research and Engineering Laboratory and the Danish National Space Centre (DNSC-DTU). As part of the IceBridge Arctic 2009 Mission, an overflight of the GreenArc survey site was conducted through a collaboration between the National Oceanic and Atmospheric Administration and the NASA. This experiment was designed to sample the thickest ice of the Arctic Ocean and presented the first opportunity to compare IceBridge sea ice measurements with coincident *in situ* data (Table I). In particular, this provided the first opportunity to assess the accuracy of the University of Kansas snow radar system.

Here, we investigate the potential of the University of Kansas snow radar for routine mapping of snow depth on Arctic sea ice and present the first analysis of snow radar retrievals over level first-year (FY) ice, MY ice, and heavily deformed pressure ridges. Ice thickness estimates are derived by combining information on snow loading with freeboard data derived from the ATM laser altimeter [19] and are compared with temporally and spatially coincident *in situ* measurements. Section II describes the field survey layout and the approach taken to gather both the airborne and *in situ* data sets. A description of the algorithms used to process the radar and laser data sets is provided in Section III. Section IV provides a comparative analysis of the airborne and *in situ* data, and the snow and ice thickness results are presented; Section V provides a discussion of the results, the limitations of the experiment, and directions for future validation of airborne measurements. Finally, Section VI concludes with a summary of our key findings and the advancements provided by IceBridge in terms of our observational capabilities over sea ice.

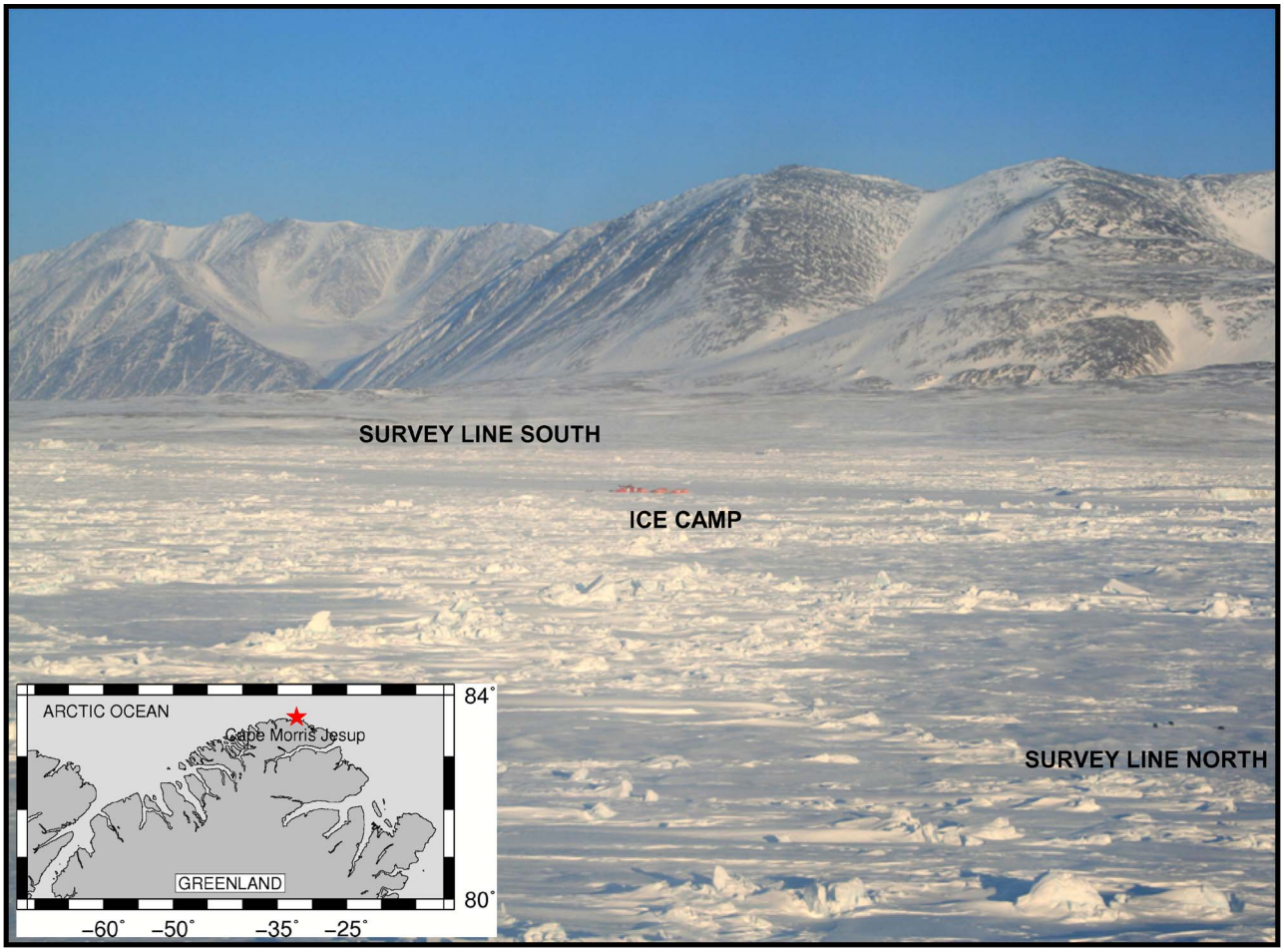

Fig. 1. Digital photograph of the survey location on fast ice north of Cape Morris Jesup, Greenland. The southern and northern ends of the survey line are indicated, as well as the red tents of the ice camp itself. Inset shows survey location (red star) off the northern coast of Greenland.

II. Data Description

A. Experiment Layout

The experiment was conducted on fast ice north of Gertrud Rask Land, Greenland on April 25, 2009 (Fig. 1). An airborne survey of the sea ice was conducted from an altitude of 490 m at a speed of ∼130 m/s on the NASA P-3 aircraft, during which the ATM, University of Kansas snow radar system, and a digital camera system were operated (see Sections II-B–D for further details). The aircraft departed Thule Air Force Base, Greenland at 11:16 UTC, before transiting along the Nares Strait and the north-western coast of Greenland, en route to the GreenArc survey area (Fig. 1).

The *in situ* survey consisted of three components: 1) a 2-km linear transect oriented in a north-south direction (Fig. 2(a), red line), along which snow depth and sea ice thickness were measured; 2) a set of drill holes located on level, undeformed FY ice parallel to the aircraft runway (Fig. 2(a), black diamonds), where direct measurements of sea ice freeboard and thickness were recorded; and 3) a set of four snow pits excavated adjacent to the main survey line (Fig. 2(a), pink dots), where snow density and snow pack stratigraphy were recorded. Concurrent with the *in situ* data collection, the P-3 conducted an areal survey of the local sea ice area (Table I). This survey consisted of six parallel flight lines oriented in a north-south direction (Fig. 2(a), blue lines) above the main *in situ* transect, where each flight line (including turns) took approximately 10 min to complete. An initial composite of the ATM swath elevation data provided an estimate of surface roughness, derived from the surface elevation and standard deviation of surface elevation measurements, at an approximate scale of 10 m. This was used to delineate three distinct sea ice provinces. Following Herzfeld *et al.* [20], a sea ice province is defined as an area that is homogeneous with respect to surface structure and the ice types it contains. The three ice provinces, denoted by background color, are shown in Fig. 2(a): undeformed level FY ice (Fig. 2(a), green), MY ice (Fig. 2(a), white), and heavily deformed ice including thick pressure ridges, rafted blocks, and a tabular iceberg confined by the ice pack (Fig. 2(a), orange). In addition to digital photography taken on the sea ice itself (Fig. 1), local ice conditions were recorded using the airborne digital camera system [Fig. 2(b)].

B. In Situ Data Collection

Snow depth and total ice thickness were measured at 5-m intervals along the ∼2 km linear transect, which was oriented in a north-south direction across undeformed level FY ice, transitioning to MY ice, and heavily deformed ice. Snow thickness was measured using a ski pole with a tape measure attached, while a Geonics EM-31 MKII electromagnetic ground conductivity meter (hereinafter referred to as the "EM31") was used to

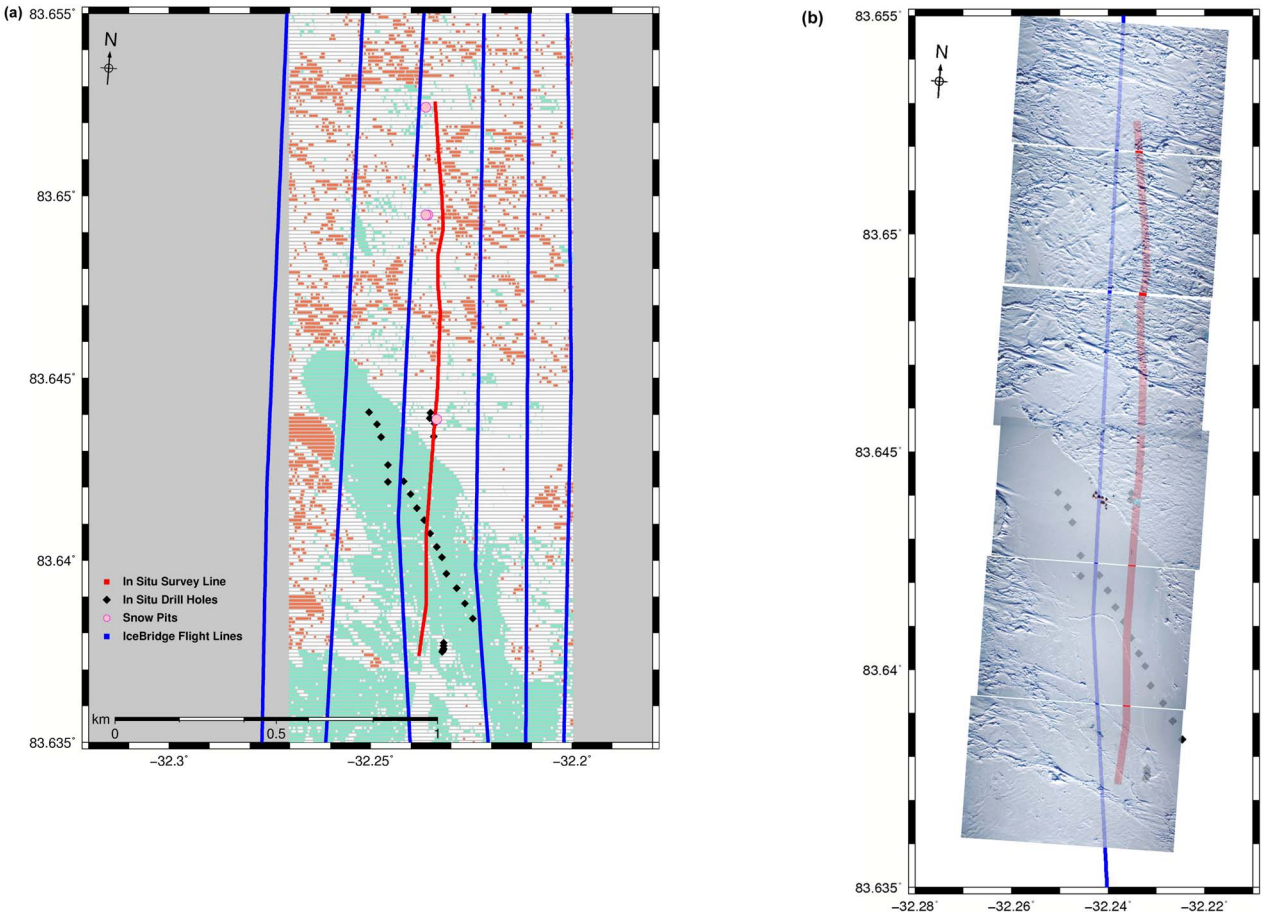

Fig. 2. (a) Detailed mapping of *in situ* survey layout (red line) with snow pits (pink dots), drill holes (black diamonds), and aircraft ground tracks (blue). Ice type, denoted by background color and derived from ATM data, consisted of undeformed level first-year ice (green), multiyear ice (white), and heavily deformed ice with thick ridges and a tabular iceberg confined by the ice pack (orange). The third flight line from the left (flight line #3) was the closest to the *in situ* transect. (b) Digital photography collected along flight line 3 indicating surface roughness in survey area; survey line and drill holes denoted as for 2a.

measure snow plus ice thickness. The EM31 instrument works by measuring the large contrast between the apparent conductivity of sea ice and the underlying higher salinity seawater (see Haas [21] for further details). The snow depth measurements were subtracted from the EM31 measurements to estimate total sea ice thickness. The EM31 system provides sea ice thickness with an accuracy of ∼0.1 m over level ice [21], [22]. Field measurements show a limitation in the penetration depth of ∼7.5 m in thicker undeformed MY ice due to the system's signal strength [23]. The EM31 is not well suited for thickness measurements in regions of heavily deformed ice due to issues associated with instrument footprint and substrate porosity. Global positioning system (GPS) locations were also recorded every 100 m. A total of 356 individual *in situ* measurements were made along the survey line.

On the undeformed level ice of a refrozen lead (Fig. 2(a), green data points), sea ice freeboard and total ice thickness were measured at a set of drill holes (Fig. 2(a), black diamonds). The EM31 instrument was also calibrated at these drill hole sites and the EM31 ice thickness measurements verified. In addition, a set of four snow pits were excavated along the survey transect (Fig. 2(a), pink dots) where snow density was recorded. A combined total of 386 EM31 ice thickness measurements and 356 snow depth measurements were collected over the entire survey area.

C. Airborne Laser Altimetry

ATM laser altimetry data [18] were collected over the survey region to define the sea ice surface topography. The ATM is a scanning laser altimeter which operates at a wavelength of 532 nm and measures surface elevation with respect to the WGS84 reference ellipsoid, to an accuracy of ∼0.1 m, by incorporating measurements from GPS receivers and inertial navigation system attitude sensors [18]. Here, we use the IceBridge ATM L1B Qfit Elevation data [24], which were collected by the ATM2 instrument operating at a 15.3° scan angle. From a flight altitude of 490 m, this resulted in ∼1 m footprints, distributed ∼3 m apart in the along-track direction and 1–5 m apart in the across-track direction [18], in conically scanned swaths ∼268 m wide in the across-track direction, consistent with the geometry calculated by Connor *et al.* [25]. For a depiction of the ATM scan geometry, see Fig. 1 in Farrell *et al.* [26].

D. Snow Radar

An ultrawideband FMCW radar has been developed at the Center for Remote Sensing of Ice Sheets (CReSIS) at the University of Kansas to measure snow depth on sea ice [17]. The snow radar, operating from 2.5 to 7 GHz, was used to measure snow-pack thickness in the survey area [17]. With 4.48 GHz of useable bandwidth, the snow radar had a pulse-limited footprint approximately 16 m wide in the across-track direction by 15 m in the along-track direction. The snow radar had a 1-m along-track sampling rate and a range resolution of ~0.05 m in the snow pack [17]. Here, we use the IceBridge Snow Radar L1B Geolocated Radar Echo Strength Profiles [27], which contain radar backscatter measurements of snow depth. The raw data has been processed to an intermediate stage following four coherent integrations, high-pass filtering in the along-track direction, and pulse compression using a fast Fourier transform. A Hanning window is applied to each received waveform for range sidelobe suppression, a Wiener filter is used to reduce speckle, and an aircraft altitude correction is applied [17]. Derivation of actual snow depth required further postprocessing and is described in Section III-B below.

E. Photography

The Continuous Airborne Mapping By Optical Translator (CAMBOT) nadir-looking digital camera system was used to collect photographs of the ice surface along each flight trajectory. Each CAMBOT image file is associated with an ASCII text file that includes the time of acquisition, latitude and longitude of the center of the nadir view, aircraft altitude above the WGS84 reference ellipsoid, and aircraft pitch, roll, and heading from an ATM-linked GPS/IMU systems. We used the IceBridge CAMBOT L1B Geolocated and Orthorectified Images [28] first to identify the ice camp itself and the flight lines closest to the *in situ* survey line, then to characterize sea ice morphology in the survey region [Fig. 2(b)].

III. Data Processing

A. ATM Processing and Freeboard Adjustment

Local sea surface height, estimated from the elevation of nearby leads, is usually subtracted from ice floe elevation measurements to derive sea ice freeboard. An absence of leads in the fast-ice survey region prevented a direct measurement of local sea surface height. Initially, it was therefore not possible to estimate sea ice freeboard using the airborne measurements alone. Subtracting a model of the geoid, which represents the theoretical shape of the sea surface at rest, in the absence of oceanic or atmospheric circulation, from the ice floe elevations, provides a first approximation of sea ice freeboard. Here, the EGM2008 geoid model [29] was removed from the ATM elevation data, resulting in a "pseudo freeboard," that is not corrected for instantaneous sea surface conditions (e.g., tides, currents, and atmospheric pressure). A comparison of 16 direct *in situ* measurements of sea ice freeboard with a subset of ATM data (9909 data points) across level FY ice [green data points, Fig. 2(a)] revealed an offset of 0.307 m between the mean ATM pseudo freeboard (0.570 m) and the mean freeboard measured *in situ* (0.263 m). This offset represents the difference between the instantaneous sea surface conditions and the geoid due to dynamic topography at the time of the survey. The empirically derived offset was then applied as a sea surface height correction to the entire ATM surface elevation data set to obtain corrected ATM sea ice freeboard estimates across the GreenArc survey region.

Analysis of the subset of ATM data gathered over the level FY ice surface of a refrozen lead (Fig. 2(a), green data points) also provides an opportunity to conduct an independent assessment of the accuracy of the laser altimetry over a level surface with constant reflectivity. The ATM data collected over the level FY ice were placed onto a grid with a latitudinal spacing of 2.5 m and a longitudinal spacing of 25 m. On average, this gridding procedure resulted in 1.4 individual ATM data points per grid cell. The standard deviation (σ) of the altimetry elevations across the level FY ice was 0.047 m, compared to a standard deviation of 0.015 m for the measured freeboards, reflecting a combination of instrument noise associated with the ATM measurements, as well as sensitivity to small-scale surface roughness that may have been undersampled by the limited *in situ* freeboard survey. The ~0.05-m estimated accuracy of the ATM data is consistent with other estimates of ATM single shot elevation error (e.g., 18).

As mentioned earlier, the corrected ATM surface elevation data were used to derive sea ice freeboard across the survey region. To facilitate later combination with snow depths derived from the snow radar system, the freeboard data were placed onto a grid approximately 12 m by 12 m, resulting in an average of 46 individual measurements per grid cell. Assuming i measurements are summed to estimate mean freeboard, the standard error (for a 95% confidence interval) associated with the ATM freeboard for our survey region is

$$\varepsilon h_f = \frac{2\sigma}{\sqrt{i}} \tag{1}$$

where h_f is the snow–ice freeboard (defined as the elevation of sea ice plus accumulated snow above local sea level), σ is the standard deviation of the freeboard measurements over the level refrozen lead surface, and i is the mean number of data points per grid cell (i.e., for $i = 46$, $\varepsilon h_f = 0.014$ m).

B. Radar Processing and Derivation of Snow Thickness

Snow depth retrievals from the snow radar are accomplished first by detection of the air–snow and snow–ice interfaces within the radar signal, and second, by the determination of the spatial distance between the two. The dielectric constant of snow is ~1.5 for a snow density of 264 kgm^{-3} (mean snow density measured *in situ*), while the dielectric constant for ice is about twice that at ~3.1 [30]. The difference between the dielectric constants of air, snow, and sea ice results in two maxima in the radar return, corresponding to the air–snow and snow–ice interfaces. The return from the snow–ice interface is typically the larger of the two, although the magnitude of return power will vary depending on the roughness of the interfaces. To increase the signal-to-noise ratio (SNR) and enhance detection of the two interfaces, along-track waveform stacking is performed using 20 contiguous waveforms for each stack. Given the sampling frequency of the snow radar (~1 m), for each radar footprint, waveforms approximately ±10 m

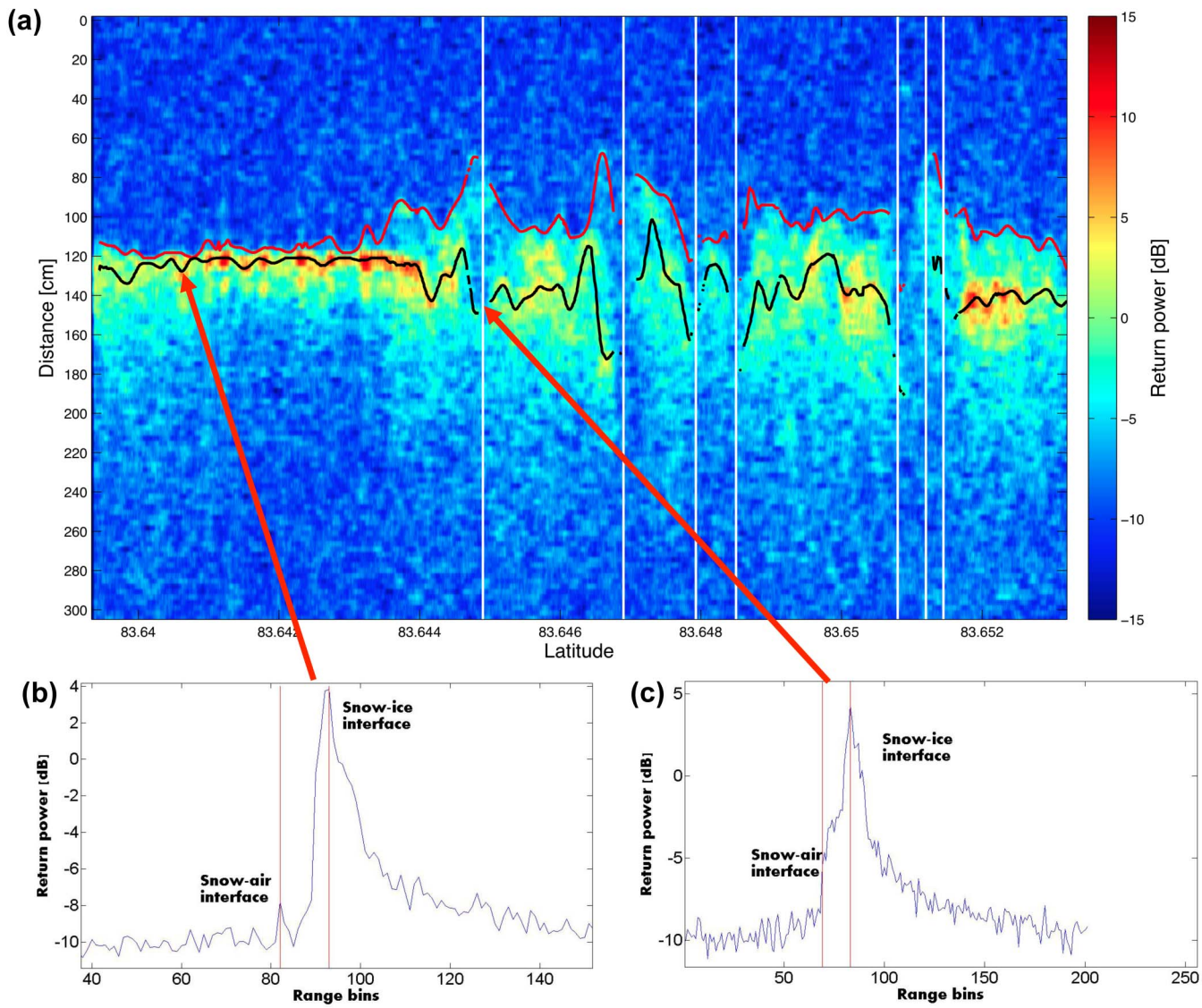

Fig. 3. (a) Processed snow radar echogram with air/snow (red) and snow/ice (black) interfaces indicated. Vertical white lines indicate where temporary loss of the snow radar signal along track. (b) Individual snow radar return with clearly defined peaks in return power at the air–snow and snow–ice interfaces. (c) Individual snow radar return with an indistinct air–snow interface.

about that footprint are included in the waveform stack. The vertical bin size of a radar waveform is approximately 0.1 ns, corresponding to a theoretical range resolution of about 0.03 m. The noise level of each radar waveform is calculated by taking the mean $(\overline{N})$ and standard deviation (σ_N) of the return power (P_r [in units of dB]) in 200 bins located at least 5 m above the point of maximum power.

Due to the relatively low difference between the dielectric constants for air and snow, as well as surface roughness effects, the air–snow interface can be difficult to detect; a threshold is set to identify the top of the snow layer within the radar return by detecting the first point where P_r satisfies the conditions

$$P_r \geq (\overline{N} + x\sigma_N) \tag{2}$$

$$\overline{P_r} \geq (\overline{N} + x\sigma_N) \tag{3}$$

where $\overline{P_r}$ is the average power in the six range bins below the air–snow interface. Together these two conditions help identify the air–snow interface and distinguish the snow layer from random noise spikes. A threshold (x) is set so as to distinguish the surface return from the background noise. Visual inspection of a radar echogram typical of the survey area suggests that a value of $x = 2.3$ is a satisfactory threshold to distinguish the onset of the surface return. The air–snow interface is then defined as the local peak in return power following this initial threshold. In many cases, surface and volume scattering cause the radar waveform to become diffuse, such that the expected local maximum corresponding to the mean air–snow interface cannot easily be distinguished. In these cases where no local maximum can be identified, the air–snow interface is set to the first point where P_r satisfies the condition

$$P_r \geq (\overline{N} + 2.8\sigma_N). \tag{4}$$

This condition is based on an analysis of a subset of quasispecular returns where the air–snow interface can be clearly identified. For diffuse returns, an empirically derived value of

TABLE II
MEAN, MODE, AND STANDARD DEVIATION (m) OF SNOW DEPTH MEASURED *IN SITU* AND DERIVED FROM THE SNOW RADAR, ACROSS THE LEVEL FIRST-YEAR ICE SITE

Parameter	# Data Points	Mean	Mode	Standard Deviation
Measured Snow Depth (m)	184	0.095	0.045	0.103
Snow Radar Snow Depth (m)	1764	0.096	0.057	0.070

2.8 limits the return power from the snow-air interface so that it is less than or equal to the power which may be expected from a quasispecular surface, but that is also above the background noise level. The snow–ice interface is subsequently defined as the local maximum of P_r following the air–snow interface. Due to a larger difference between the dielectric constants of snow and ice, the snow–ice interface is easier to detect.

In certain cases (e.g., pressure ridges), the return power value for the estimated snow–ice interface (P_{si}) may fall within the noise level. In these cases, detection of the air–snow and snow–ice interfaces becomes impossible. We define a quality factor (Q) to determine the quality of the data and its viability for identification of the air–snow and snow–ice interfaces

$$Q = \left| \frac{P_{si} - \overline{N}}{\sigma_N} \right|. \tag{5}$$

We find that diffuse radar returns originating over heavily ridged ice were typically associated with a quality factor $Q < 6$, such that the return power was too low to accurately define the air–snow and snow–ice interfaces. In these cases, the radar return was indistinguishable from background noise, and snow depth could not be determined. In this study, 20% of the radar data had $Q < 6$, and these data were associated with returns over heavily ridged ice (see Section IV-A for further details).

Once the air–snow and snow–ice interfaces are established in the time domain, they are converted into distance to determine snow depth. Range bins in the time domain are converted to snow depth by multiplying by the speed of light in the snow pack. The speed of light in the snow pack, c_s, is defined as

$$c_s = \frac{c}{n_s} \tag{6}$$

where c is speed of light in vacuum, and n_s is the snow index of refraction. Following [30], n_s is estimated from the snow density (ρ_s) as

$$n_s = \sqrt{(1.0 + 2.0\rho_s)}. \tag{7}$$

For this study, ρ_s is 0.264 gcm^{-3} and is based on the mean snow density measured *in situ* at snow pits adjacent to the survey transect line.

Oversampling by the snow radar (1-m sampling interval with a ~15-m footprint size) allows for statistical smoothing and noise reduction of the airborne snow depth data. From a locally weighted "robust linear regression" technique, initial estimates for the air–snow and snow–ice interfaces, as described above, are smoothed to reduce the impact of outliers in the snow depth detection scheme. An along-track smoothing of 40 m was applied to the snow radar data.

Fig. 3(a) shows the air–snow (red) and snow–ice (black) interfaces identified in the radar echogram along a portion of flight line 3 that is nearly coincident with the *in situ* survey and a typical return with clearly defined peaks at the two interfaces [Fig. 3(b)]. At some along-track locations, the SNR was too low (i.e., $Q < 6$) such that it was not possible to define the air–snow and/or snow–ice interfaces [Fig. 3(c)]. These locations (e.g., 83.645° N) are identified in Fig. 3(a) by vertical white lines. Table II indicates the results of a comparison between snow depths derived by the snow radar across the level FY ice (refrozen lead) and those measured *in situ*. Both techniques yielded a mean snow depth of ~0.1 m, with a modal snow depth of 0.05–0.06 m. While this comparison comprises only a portion of the total snow depth data set, these initial results across the level FY ice demonstrate the successful identification of the air–snow and snow–ice interfaces by the snow radar algorithm and provide a first estimate of the accuracy of the snow radar (~0.01 m) on level FY ice with a thin snow cover.

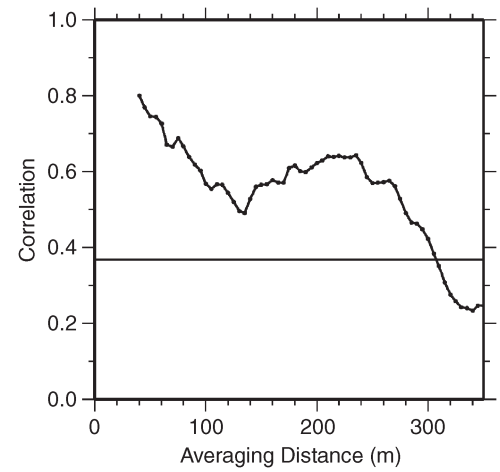

Fig. 4. Correlation computed as a function of distance using *in situ* snow depth data averaged to 40 m.

IV. RESULTS

The third aircraft overpass [Fig. 2(a)] was the closest flight line to the *in situ* transect. To examine the capabilities and limitations of the snow radar over level, MY and heavily deformed ice, we conducted a more detailed comparison between snow depths derived from the snow radar along flight line #3 and those measured *in situ*.

Since the aircraft and *in situ* survey lines do not directly overlap and are offset by 50–100 m along track, we first derive the correlation length scale of snow depth in the survey area to assess the comparison between the *in situ* and airborne measurements. We averaged the *in situ* data to 40 m along the transect (i.e., running averages of 8 *in situ* measurements) to simulate the 40-m radar data (see Section III-B). Next, we computed the autocorrelation function of snow depth in the survey area as a function of distance (Fig. 4). We find that for distances of 50–100 m (i.e., the separation between the

TABLE III
MEAN, MODE, STANDARD DEVIATION, AND MAXIMUM VALUE (m) OF SNOW DEPTH MEASURED *IN SITU* ALONG THE SURVEY LINE AND SNOW DEPTH DERIVED FROM THE SNOW RADAR ALONG FLIGHT LINE NUMBER 3

Parameter	# Data Points	Mean	Mode	Standard Deviation	Maximum
Measured Snow Depth (m)	356	0.257	0.060	0.263	1.080
Snow Radar Snow Depth (m)	2113	0.249	0.080	0.138	0.995

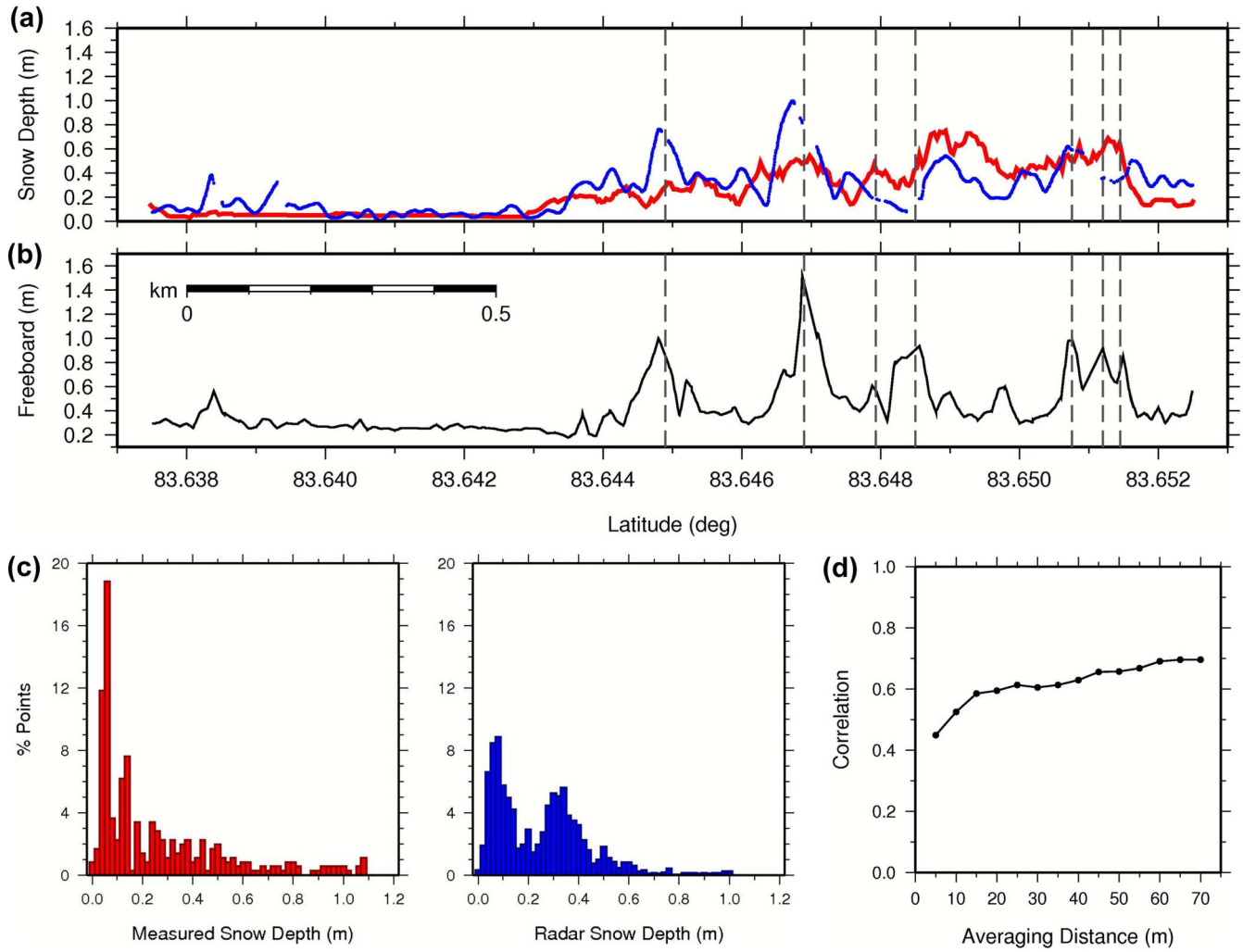

Fig. 5. (a) Profiles of snow depth measured *in situ* (red) and derived from the snow radar (blue). Vertical dashed lines indicate the temporary loss of the snow radar signal along track. (b) Corrected ATM freeboard along flight line 3 (black), with vertical dashed lines plotted at locations along track where temporary loss of the snow radar signal occurs. (c) Distributions of snow depth measured along survey line (red) and derived from the snow radar along flight line 3 (blue), using 0.02 m bins. (d) Correlation between snow depth measured *in situ* and derived from the snow radar versus along-track averaging length, from 5 m to 70 m.

aircraft line and surface transect), we can expect a maximum correlation between the snow radar and *in situ* data sets to be between 0.57 and 0.75. We find that beyond 300 m, the *in situ* snow depth measurements are no longer correlated (i.e., correlation drops below the e^{-1} level, indicated by a horizontal black line in Fig. 4).

A. Snow Depth

An examination of the *in situ* snow depth measurements along the survey transect revealed a mean snow depth of 0.26 m, while the average snow thickness derived from the snow radar system was 0.25 m (Table III). The maximum snow thickness measured by both techniques was ~1 m, although the standard deviation of the *in situ* measurements (0.26 m) was greater than those derived from the snow radar (0.14 m). The difference in the standard deviation is due to the along-track sampling (i.e., the effective footprint size). While the *in situ* data were collected every 5 m along track, the snow radar data were averaged to 40 m. Thus, the standard deviation reflects surface roughness at two length scales (5 m and 40 m). These results show that the snow radar can be used to successfully retrieve accurate snow depths and may be used in conjunction with sea ice freeboard derived from the ATM data to estimate sea ice thickness.

An assessment of the snow depth profile along the survey lines [Fig. 5(a)] reveals that the major deviations between snow radar snow depth (blue curve) and *in situ* measurements (red curve) occurred at ridge locations (vertical dashed lines) determined from the ATM freeboard height (Fig. 5(b), black curve); examples occur at 83.6385° N, 83.6448° N, and 83.6470° N. The along-track profiles do however agree in the overall pattern of snow depth across the survey illustrating lighter snow cover (∼0.05–0.1 m) over the level FY ice at the southern end of the survey and a deeper snow pack (∼0.25–0.6 m) at the northern end of the survey area.

Fig. 5(c) compares the snow thickness distributions derived from a segment of flight line #3, between 83.6375° N and 83.6525° N, (blue) and the surface transect (red). The major mode of both distributions occurred at 0.06–0.08 m which indicates the average snow depth on the level FY ice at the southern section of the survey. A secondary mode at ∼0.34 m in the snow radar snow thickness distribution does not occur in the *in situ* data (see Section V for further discussion). We also computed the correlation between snow depths measured *in situ* and those derived from the snow radar, with respect to an along-track averaging length [Fig. 5(d)]. A previous study conducted by Markus *et al.* [31] comparing airborne and *in situ* measurements of snow depth found that spatial averaging of the *in situ* data in the order of 50–250 m was required for comparison with airborne data gathered over a larger scale. Similar to results of Markus *et al.* [31], we found that along-track averaging of the *in situ* data was necessary for comparison with airborne measurements. We find a strong correlation between the data at averaging lengths greater than 25 m, with an average correlation coefficient of $R = 0.62$. A maximum correlation of 0.7 is reached at a length scale of 55–60 m. This result is consistent with the autocorrelation of the *in situ* data (Fig. 4), which suggested that we may expect a maximum correlation between the two data sets between 0.6 and 0.75 given the 50–100 m offset between survey line locations.

A map of snow depths (Fig. 6) shows good agreement between the airborne snow thicknesses and those measured *in situ*. In Fig. 6, the snow depth data measured *in situ* and from the airborne system are overlaid on sea ice freeboard to allow delineation between level and deformed sea ice provinces. The thinnest snow was found on the level refrozen lead, while thicker snow depths were measured in the snow drifts that accumulated on the leeward side of pressure ridges. Indeed, differences in the along-track snow depths show peaks in snow radar snow depths where the aircraft crossed ridges (indicated by high freeboard values, in Figs. 5(b) and 6), while the survey transect did not, consistent with the along-track profiles in Fig. 5(a) and (b).

B. Sea Ice Thickness

We combined the ATM derived sea ice freeboard described in Section III-A, with the airborne snow depth measurements to estimate sea ice thickness in the survey area. The thickness of a sea ice floe, h_i, is calculated by assuming local hydrostatic balance as follows:

$$h_i = \frac{\rho_w}{\rho_w - \rho_i} h_f - \frac{\rho_w - \rho_s}{\rho_w - \rho_i} h_s \tag{8}$$

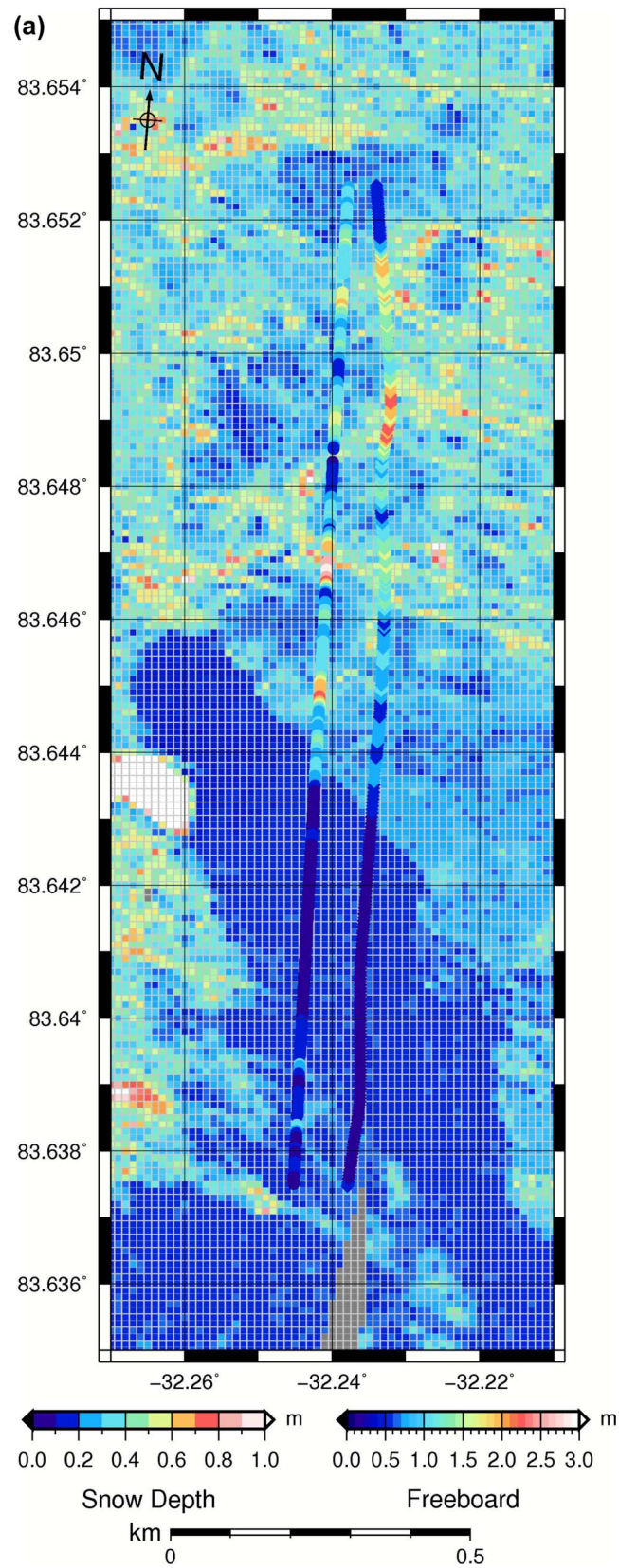

Fig. 6. Map showing snow depth measured *in situ* (diamonds, right) and derived from snow radar (circles, left) along flight line 3. Snow measurements are overlaid on sea ice freeboard derived from ATM data.

TABLE IV
AVERAGE VALUE AND ESTIMATED UNCERTAINTY ASSOCIATED WITH THE FIVE VARIABLES OF THE SEA ICE THICKNESS EQUATION [SEE (8)]

Parameter	Average Value	Source	Estimated Uncertainty	Source
Snow-ice Freeboard (h_f)	0.414 m	Mean ATM freeboard	0.014 m	As derived in equation (1)
Snow Depth (h_s)	0.250 m	Mean snow depth measured by radar	0.050 m	Table 1
Ice Density (ρ_i)	914.3 kgm^{-3}	Mean isostatic in situ first-year ice density	7.0 kgm^{-3}	Standard deviation of isostatic in situ first-year ice density
Water Density (ρ_w)	1023.9 kgm^{-3}	Wadhams et al. [24]	0.5 kgm^{-3}	Wadhams et al. [24]
Snow Density (ρ_s)	264.3 kgm^{-3}	Mean snow density measured in situ	7.9 kgm^{-3}	Standard deviation of in situ snow density measurements

TABLE V
MEAN, MODE, AND STANDARD DEVIATION (m) OF ICE THICKNESS MEASURED *IN SITU* AND DERIVED FROM THE COMBINED ICEBRIDGE DATA SET. THE ESTIMATED ERROR ($\varepsilon_{\rm est}$) ASSOCIATED WITH THE *IN SITU* SEA ICE THICKNESS MEASUREMENTS IS BASED ON THE ACCURACY OF THE EM-31 OVER LEVEL SEA ICE ONLY (E.G., HAAS *ET AL*, [21]), WHILE FOR THE ICE THICKNESS DERIVED FROM THE ICEBRIDGE DATA $\varepsilon_{\rm est}$ IS BASED ON THE PROPAGATION OF ERROR SOURCES FOR THE VARIABLES USED IN THE ICE THICKNESS CALCULATION [SEE (9)]

Parameter	# Data Points	Mean	Mode	Standard Deviation	εest
Measured Ice Thickness (m)	288	2.628	2.000	0.941	0.100
IceBridge Ice Thickness (m)	386	2.575	2.100	0.705	0.395

where ρ_w, ρ_i, and ρ_s are the density of water, ice, and snow, respectively, h_s is snow depth, and h_f is the snow–ice freeboard and is the elevation of sea ice, plus accumulated snow, above local sea level. To derive the sea ice thickness from the airborne data, we assume a water density (ρ_w) of 1023.9 kgm^{-3} following Wadhams *et al.* [32]. We apply an ice density (ρ_i) of 914.3 kgm^{-3}, the average $(n = 20)$ *in situ*, isostatic ice density derived from ice freeboard and thickness measurements gathered on the undeformed FY ice of the refrozen lead [black diamonds, Fig. 2(a)] We apply a snow density (ρ_s) of 264.3 kgm^{-3}, the average density measured in snow pits adjacent to the survey line [pink dots, Fig. 2(a)]. For a more detailed background on airborne and other techniques for measuring sea ice thickness, see Wadhams [33]. We gridded the IceBridge sea ice thickness data set using grid cells that measured approximately 25 m by 25 m, to allow for later comparison with the discrete *in situ* data points.

Next, we consider the uncertainty associated with the five variables in the ice thickness equation, h_f, h_s, ρ_w, ρ_i, and ρ_s, (8) to determine the uncertainty in total sea ice thickness estimated from the combined IceBridge data set. For each variable, the average value and its associated uncertainty are provided in Table IV. Assuming the variables are uncorrelated, the uncertainty in the ice thickness estimate, ε_{hi}, can be evaluated using a propagation of errors following Equation 4 in [14] for laser altimetry

$$\begin{aligned}\varepsilon_{hi}^2 = &\varepsilon_{hf}^2\left(\frac{\rho_w}{\rho_w-\rho_i}\right)^2 + \varepsilon_{hs}^2\left(\frac{\rho_s-\rho_w}{\rho_w-\rho_i}\right)^2\\ &+\varepsilon_{\rho s}^2\left(\frac{h_s}{\rho_w-\rho_i}\right)^2 + \varepsilon_{\rho w}^2\left(\frac{-\rho_i h_f+(\rho_i-\rho_s)h_s}{(\rho_w-\rho_i)^2}\right)^2\\ &+\varepsilon_{\rho i}^2\left(\frac{\rho_w h_f-(\rho_w-\rho_s)h_s}{(\rho_w-\rho_i)^2}\right)^2. \qquad (9)\end{aligned}$$

The uncertainty in snow depth, ε_{hs}, is the largest contribution to the ice thickness error. The analysis indicates an uncertainty (ε_{hi}) in the IceBridge ice thickness estimates of 0.395 m, for data collected in the GreenArc survey area (Table V).

The EM31 system was used to measure sea ice thickness along the survey transect, on FY ice along the refrozen lead, and at the nearby snow pit sites. Haas [21] estimates that the typical accuracy of EM31 measurements over level ice is ~0.1 m. The limitations of the system in heavily deformed ice zones, due to unconsolidated ice in thick pressure ridges with unconstrained porosity, prevents measurements of ice with thicknesses greater than ~7.5 m [23] (see Section II-B for more details). Of the 386 individual ice thickness measurements collected using the EM 31 instrument, 288 estimates less than 7.5 m were retained. For comparison with these EM31 ice thickness measurements, the 25-m gridded IceBridge thickness estimates were interpolated to the *in situ* measurement locations using bicubic interpolation. The comparison in Table V shows that there is excellent agreement between the EM31 ice thickness results and those derived independently from the airborne data. The EM31 instrument recorded a mean ice thickness of 2.63 m, with a standard deviation of 0.94 m, while a mean ice thickness of 2.58 m with a standard deviation of 0.71 m was recovered from the airborne system. Average ice thickness estimated from the EM31 and airborne systems therefore agrees to within 0.05 m. The standard deviation indicates the variability of sea ice thickness across the survey area.

The sea ice thickness distributions [Fig. 7(a)] indicate a modal ice thickness of 2.0 m and 2.1 m for the *in situ* and airborne data, respectively, which represents the thickness of level ice in the survey area. Indeed, directly drilled measurements of ice thickness across the underformed level FY ice [black diamonds, Fig. 2(a)] indicated an average ice thickness of

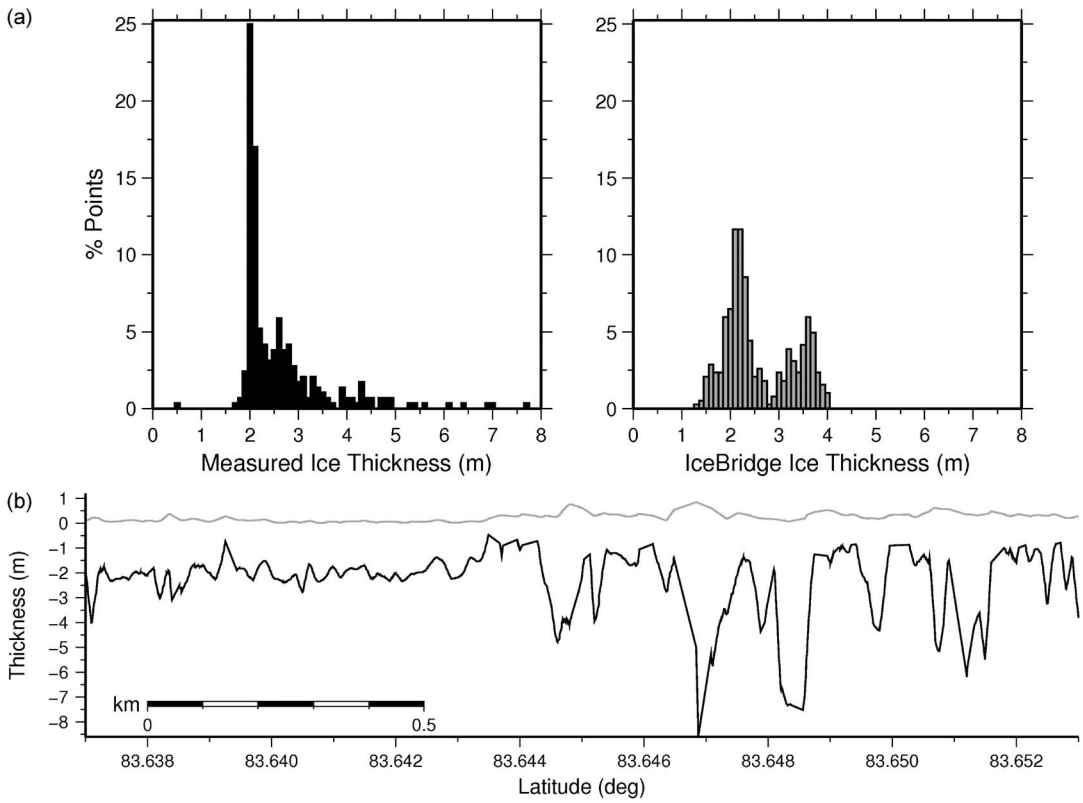

Fig. 7. (a) Distributions of the measured ice thickness (black) and the ice thickness derived from the combined IceBridge data set (gray), using 0.1 m bins. (b) Cross-section of the along-track snow depth (gray line) and ice thickness (black line) derived from the IceBridge instrument suite.

2.1 m. A difference in modal thickness between the IceBridge and EM31 results of 0.1 m demonstrates that the retrieved ice thickness distributions are accurate over level ice and falls within the uncertainties of both methods. A secondary mode at 3.6 m in the IceBridge data is the average thickness of MY ice and demonstrates the capability of the IceBridge retrieval methods to provide ice thickness estimates over MY ice floes despite the presence of pressure ridges. Finally, Fig. 7(b) shows a typical cross-section of the along-track snow depth (gray line) and ice thickness (black line) derived from the IceBridge airborne instruments over the Green Arc survey.

V. Discussion

There is excellent agreement between the snow depths and ice thicknesses derived from the IceBridge data and the *in situ* GreenArc measurements when averaged over the survey region. The *in situ* measurements revealed that mean snow depth and ice thickness were 0.26 m and 2.63 m, respectively. The average snow thickness derived from the University of Kansas snow radar system was 0.25 m (Table III), while mean ice thickness was estimated to be 2.58 m (Table V), illustrating that the snow radar system can accurately retrieve snow depth and can be combined with freeboard data to derive ice thickness. A 0.1-m difference between IceBridge and EM31 measurements of modal ice thickness demonstrates that the retrieved ice thicknesses are particularly accurate across level ice. We estimated an uncertainty of ∼0.40 m (Table V) associated with the IceBridge sea ice thickness estimates in the GreenArc survey area.

Further consideration of differences between the *in situ* and airborne snow and ice thickness distributions [Figs. 5(c) and 7(a)] is however required. The bimodal distributions of the IceBridge snow and sea ice thickness data suggest two distinct ice types in the survey region, consistent with the undeformed level FY ice type at the southern end of the transect and MY ice at the northern end of the transect [Fig. 2(a) and (b)]. There was excellent agreement between airborne and *in situ* measurements across level ice (e.g., see the along-track snow depths between 83.6375° N and 83.6435° N, Fig. 5(a), and Table II). Larger differences were however observed in the MY ice. The snow depth profile revealed deviations of ∼0.2–0.6 m between airborne snow depths and the *in situ* measurements, particularly at pressure ridges [e.g., at 83.645° N and 83.647° N, Fig. 5(a)]. Moreover, a secondary mode at 3.6 m was recorded in the airborne ice thickness distribution [Fig. 7(a)], indicating the average thickness of MY ice in the survey region, but was not observed in the EM31 thickness measurements. An offset of 50–100 m between the survey line and the closest airborne overpass precludes a one-to-one comparison between the airborne and *in situ* data. Further analysis revealed that differences observed in the snow and ice thickness distributions were due to sampling differences in the MY ice, wherein the aircraft crossed a number of thick pressure ridges [indicated by vertical dashed lines in Fig. 5(b)] that were not covered by the *in situ* survey transect [Fig. 2(a)]. Additional reasons for deviations between measurements over the MY ice include the differences in the along-track sampling of the airborne (∼1 m) and *in situ* (∼5 m) data, difficulty in calculating snow thickness at the apexes of heavily ridged ice using the snow

radar system [e.g., vertical white (dashed) lines indicating data dropouts where the quality factor (Q) is low, Fig. 3 (5b)], and the limitations of the EM31 instrument which undersamples ridge thickness.

Although we have presented the first assessment of IceBridge data and have verified the results through comparison with coincident *in situ* measurements, a number of limitations to the analysis exist. Due to partial spatial coincidence between the two data sets, potential errors in the snow radar algorithm remain difficult to define, and the 2-km long GreenArc transect represents a limited data set with respect to ice type.

Given these findings, we now provide a number of recommendations for future validation of airborne data via *in situ* field measurements. The survey performed during the GreenArc 2009 campaign was opportunistic in character and was conducted in just one day. An extended field campaign would allow for longer *in situ* survey lines and the collection of data over a wider variety of ice types and sea ice morphologies. This would provide additional data for statistical analysis, allowing a more detailed assessment of errors in the IceBridge data set. Ideally, *in situ* survey lines would be at least 5 km in length and would cover a variety of ice types and snow stratigraphies, such that they would be representative of the region beyond the immediate survey area. Indeed, in April 2011, such a set of *in situ* data were gathered along a 9-km long survey line at the US Navy's Ice Expedition 2011 (ICEX 2011) ice camp. These snow and ice thickness measurements were collected across a wide range of ice types (e.g., refrozen leads, deformed and undeformed FY ice, and MY ice), in coordination with an airborne IceBridge sea ice survey. Analysis of this data will form part of a complimentary study and will enable further evaluation of the accuracy of IceBridge snow and ice thickness estimates as a function of ice type.

Direct measurements of sea ice freeboard and thickness on undeformed level ice (such as a refrozen lead with uniform snow depth) are critical, since a refrozen lead is an ideal calibration surface. Local sea surface height could usually be estimated from the elevation of nearby leads and subtracted from sea ice elevation measurements to derive sea ice freeboard. However, in the absence of leads in the survey region (such as at the GreenArc 2009 ice camp), direct measurements of freeboard at a level ice site allow the airborne laser altimeter elevation measurements to be adjusted to local sea level so that freeboard may be determined. A number of aircraft overpasses to capture both the survey line as well as the surrounding area should be considered. This ensures that not only *in situ* measurements gathered along the survey transect are captured, but any additional measurements, such as data collected at nearby calibration sites and snow pits, would also be covered within the footprint of the aircraft instrumentation, thereby maximizing return. Furthermore, overlapping ATM swaths provide an independent calibration of the pitch and roll corrections applied to the ATM elevations during postprocessing. Such a flight configuration also provides a dense data set over the survey area, improving the SNR, such that a gridded data set will be highly precise (e.g., uncertainty in ATM freeboards gathered over the GreenArc 2009 survey site was estimated at $\sim$0.01 m). Finally, both snow and ice density should be measured at the *in situ* survey site if possible, to reduce uncertainties in the final derivation of sea ice thickness from the airborne data.

VI. Summary

We have presented the first assessment of IceBridge data gathered over Arctic sea ice, via comparisons with coincident *in situ* measurements collected at the GreenArc ice camp, located on fast ice north of Greenland. Here, we have investigated the utility of IceBridge data for the retrieval of the snow and sea ice thickness of the winter ice pack. The results are the first demonstration that IceBridge data provide accurate measurements of snow and ice thickness over both level FY ice and MY ice; Analyses of the snow radar data indicate an accuracy of $\sim$0.02 m for snow depths derived over level ice. Snow depths derived from the snow radar and those collected *in situ* had a maximum correlation of 0.7 given an averaging length of $\sim$55 m. Excellent agreement ($\sim$0.05–0.1 m) between the IceBridge and EM31 estimates of mean and modal ice thickness ($\sim$2.6 m and $\sim$2.0 m, respectively) was observed. A secondary mode captured only in the IceBridge sea ice thickness distribution indicated an average MY ice thickness of 3.6 m in the survey region. Retrieval of snow depth, and hence the derivation of sea ice thickness, over heavily ridged ice was not possible using this IceBridge data set, due to a low signal-to-noise level in the snow radar returns. This accounted for $\sim$20% of the data analyzed in this study.

Until now, we have lacked a routine and systematic observation system for mapping snow depth on Arctic Ocean sea ice. A robust and sustained monitoring of snow depth would represent a major advancement in our observational capabilities of sea ice and would significantly improve the accuracy of basin-scale sea ice thickness estimates. Regional-scale mapping of snow depth on sea ice would also provide information on the interannual variability of Arctic precipitation rates. In particular, we have demonstrated that the University of Kansas snow radar represents a significant advancement in our observational capability for measuring the snow depth on sea ice. Techniques developed here to process snow radar echograms will be used to process additional IceBridge data gathered over Arctic sea ice during recent campaigns between 2009 and 2011. Development of algorithms for deriving Antarctic snow depth will form part of a complementary study where the impact of flooding of the snow pack at the snow–ice interface (e.g., [13] and [34]) will require further investigation. Combined with ATM airborne laser altimetric measurements of sea ice freeboard, the snow thickness data may be used to routinely derive Arctic ice thickness along IceBridge flight lines.

Acknowledgment

The authors thank the ATM team at NASA Wallops Flight Facility for processing the laser altimetry data and digital photography, and the University of Kansas CReSIS radar team for providing the snow radar data. Operation IceBridge data are available at http://nsidc.org/data/icebridge/index.html. The authors also thank Rene Forsberg of the Danish National Space Center (DNSC-DTU) and Leif Toudal Pedersen of the Danish Meteorological Institute (DMI) for providing the opportunity to participate in the GreenArc 2009 ice camp, as well as Jeremy Wilkinson and Susanna Hanson for assistance with the collection of *in situ* data. The authors would like to thank also

S. Martin and two anonymous reviewers for providing very helpful suggestions and comments.

REFERENCES

[1] N. T. Kurtz, T. Markus, S. L. Farrell, D. Worthen, and L. N. Boisvert, "Observations of recent Arctic sea ice volume loss and its impact on ocean-atmosphere energy exchange and ice production," *J. Geophys. Res.*, vol. 116, p. C04 015, 2011. DOI:10.1029/2010JC006235.

[2] S. L. Farrell, S. W. Laxon, D. C. McAdoo, D. Yi, and H. J. Zwally, "Five years of Arctic sea ice freeboard measurements from ICESat," *J. Geophys. Res.*, vol. 114, p. C04 008, 2009. DOI:10.1029/2008JC005074.

[3] R. Kwok, G. F. Cunningham, M. Wensnahan, I. G. Rigor, H. J. Zwally, and D. Yi, "Thinning and volume loss of the Arctic Ocean sea ice cover: 2003–2008," *J. Geophys. Res.*, vol. 114, no. C7, p. C07 005, 2009. DOI:10.1029/2009JC005312.

[4] K. A. Giles, S. W. Laxon, and A. L. Ridout, "Circumpolar thinning of Arctic sea ice following the 2007 record ice extent minimum," *Geophys. Res. Lett.*, vol. 35, p. L22 502, 2008. DOI:10.1029/2008GL035710.

[5] W. Abdalati, H. J. Zwally, R. Bindschadler, B. Csatho, S. L. Farrell, H. A. Fricker, D. Harding, R. Kwok, M. Lefsky, T. Markus, A. Marshak, T. Neumann, S. Palm, B. Schutz, B. Smith, J. Spinhirne, and C. Webb, "The ICESat-2 laser altimetry mission," *Proc. IEEE*, vol. 98, no. 5, pp. 735–751, May 2010.

[6] M. Sturm, J. Holmgren, and D. K. Perovich, "Winter snow cover on the sea ice of the Arctic Ocean at the Surface Heat Budget of the Arctic Ocean (SHEBA): Temporal evolution and spatial variability," *J. Geophys. Res.*, vol. 107, no. C10, p. 8047, 2002.DOI:10.1029/2000JC000400.

[7] D. K. Perovich, T. C. Grenfell, J. A. Richter-Menge, B. Light, W. B. Tucker, III, and H. Eicken, "Thin and thinner: Sea ice mass balance measurements during SHEBA," *J. Geophys. Res.*, vol. 108, no. C3, p. 8050, 2003. DOI:10.1029/2001JC001079.

[8] M. Sturm, J. A. Maslanik, D. K. Perovich, J. C. Stroeve, J. Richter-Menge, T. Markus, J. Holmgren, J. F. Heinrichs, and K. Tape, "Snow depth and ice thickness measurements from the beaufort and chukchi seas collected during the AMSR-Ice03 campaign," *IEEE Trans. Geosci. Remote Sens.*, vol. 44, no. 11, pp. 3009–3020, Nov. 2006.

[9] S. G. Warren, I. G. Rigor, N. Untersteiner, V. F. Radionov, N. N. Bryazgin, Y. I. Aleksandrov, and R. Colony, "Snow depth on Arctic sea ice," *J. Clim.*, vol. 12, no. 6, pp. 1814–1829, 1999.

[10] S. W. Laxon, N. Peacock, and D. Smith, "High interannual variability of sea ice thickness in the Arctic region," *Nature*, vol. 425, no. 6961, pp. 947–949, Oct. 2003.

[11] Nat. Snow Ice Data Center, Digital media D. Yi and J. Zwally, Arctic Sea Ice Freeboard and Thickness, Boulder, CO2010, Digital media.

[12] R. Kwok and G. F. Cunningham, "ICESat over Arctic sea ice: Estimation of snow depth and ice thickness," *J. Geophys. Res.*, vol. 113, p. C08 010, 2008. DOI:10.1029/2008JC004753.

[13] R. C. Willatt, K. A. Giles, S. W. Laxon, L. Stone-Drake, and A. P. Worby, "Field investigations of Ku-band radar penetration into snow cover on Antarctic sea ice," *IEEE Trans. Geosci. Remote Sens.*, vol. 48, no. 1, pp. 365–372, Jan. 2010.

[14] K. A. Giles, S. W. Laxon, D. J. Wingham, D. Wallis, W. B. Krabill, C. J. Leuschen, D. McAdoo, S. S. Manizade, and R. K. Raney, "Combined airborne laser and radar altimeter measurements over the Fram Strait in May 2002," *Remote Sens. Environ.*, vol. 111, no. 2/3, pp. 182–194, Nov. 2007.

[15] P. Kanagaratnam, T. Markus, V. Lytle, B. Heavey, P. Jansen, G. Prescott, and P. Gogineni, "Ultrawideband radar measurements of thickness of snow over sea ice," *IEEE Trans. Geosci. Remote Sens.*, vol. 45, no. 9, pp. 2715–2724, Sep. 2007.

[16] N. Galin, A. Worby, T. Markus, C. Leuschen, and P. Gogineni, "Validation of airborne FMCW radar measurements of snow thickness over sea ice in Antarctica," *IEEE Trans. Geosci. Remote Sens.*, vol. 50, no. 1, pp. 3–12, Jan. 2012.

[17] B. Panzer, C. Leuschen, A. Patel, T. Markus, and P. Gogineni, "Ultra-wideband radar measurements of snow thickness over sea ice," in *Proc. IEEE IGARSS*, Honolulu, HI, Jul. 25–30, 2010, pp. 3130–3133.

[18] W. B. Krabill, W. Abdalati, E. B. Frederick, S. S. Manizade, C. F. Martin, J. G. Sonntag, R. N. Swift, R. H. Thomas, and J. G. Yungel, "Aircraft laser altimetry measurement of elevation changes of the Greenland ice sheet: Technique and accuracy assessment," *J. Geodynamics*, vol. 34, no. 3/4, pp. 357–376, Oct./Nov. 2002.

[19] N. T. Kurtz, T. Markus, D. J. Cavalieri, W. Krabill, J. G. Sonntag, and J. Miller, "Comparison of ICESat data with airborne laser altimeter measurements over Arctic sea ice," *IEEE Trans. Geosci. Remote Sens.*, vol. 46, no. 7, pp. 1913–1924, Jul. 2008.

[20] U. C. Herzfeld, J. A. Maslanik, and M. Sturm, "Geostatistical characterization of snow-depth structures on sea ice near point barrow, Alaska—A contribution to the AMSR-Ice03 field validation campaign," *IEEE Trans. Geosci. Remote Sens.*, vol. 44, no. 11, pp. 3038–3056, Nov. 2006.

[21] C. Haas, "Dynamics versus thermodynamics: The sea ice thickness distribution," in *Sea Ice: An Introduction to Its Physics, Chemistry, Biology, and Geology*, D. N. Thomas and G. S. Dieckmann, Eds. Oxford, U.K.: Blackwell Sci., 2003, p. 402.

[22] C. Haas, S. Hendricks, H. Eicken, and A. Herber, "Synoptic airborne thickness surveys reveal state of Arctic sea ice cover," *Geophys. Res. Lett.*, vol. 37, p. L09 501, 2010.

[23] C. A. Geiger, J. Richter-Menge, S. Hendricks, C. Haas, H.-R. Mueller, T. Martin, and B. Elder, "Impact of instrument footprint from electromagnetic induction sea ice thickness retrievals," *J. Geophys. Res.*, 2011, submitted for publication.

[24] W. B. Krabill, "IceBridge ATM L1B Qfit Elevation and Return Strength, 25 April 2009," *Nat. Snow Ice Data Center*, Boulder, CO, 2009.

[25] L. N. Connor, S. W. Laxon, A. L. Ridout, W. B. Krabill, and D. C. McAdoo, "Comparison of Envisat radar and airborne laser altimeter measurements over Arctic sea ice," *Remote Sens. Environ.*, vol. 113, no. 3, pp. 563–570, Mar. 2009.

[26] S. L. Farrell, T. Markus, R. Kwok, and L. Connor, "Laser altimetry sampling strategies over sea ice," *Ann. Glaciol.*, vol. 52, no. 57, pp. 69–76, May 2011.

[27] C. Leushen, "IceBridge Snow Radar L1B Geolocated Radar Echo Strength Profiles, 25 April 2009," *Nat. Snow Ice Data Center*, Boulder, CO, 2009.

[28] W. B. Krabill, "IceBridge CAMBOT L1B Geolocated Images, 25 April 2009," *Nat. Snow Ice Data Center*, Boulder, CO, 2009.

[29] N. K. Pavlis, S. Holmes, S. Kenyon, and J. K. Factor, "An earth gravitational model to degree 2160," presented at the Geophysics Research, vol. 10, 2008, Abstract v. 10 2008 EGU2008-A-01891, SRef-ID: 1607-7962/gra/EGU2008-A-01891, EGU General Assembly 2008. [Online]. Available: http://www.geophysical-research-abstracts.net/volumes.html

[30] M. Tiuri, A. Sihvola, E. Nyfors, and M. Hallikainen, "The complex dielectric constant of snow at microwave frequencies," *IEEE J. Ocean. Eng.*, vol. OE-9, no. 5, pp. 377–382, Dec. 1984.

[31] T. Markus, D. J. Cavalieri, A. J. Gasiewski, M. Klein, J. A. Maslanik, D. C. Powell, B. B. Stankov, J. C. Stroeve, and M. Sturm, "Microwave signatures of snow on sea ice: Observations," *IEEE Trans. Geosci. Remote Sens.*, vol. 44, no. 11, pp. 3081–3090, Nov. 2006.

[32] P. Wadhams, W. Tucker, W. Krabill, R. Swift, J. Comiso, and N. Davis, "Relationship between sea ice freeboard and draft in the Arctic basin, and implications for ice thickness monitoring," *J. Geophys. Res.*, vol. 97, no. C12, pp. 20 325–20 334, 1992.

[33] P. Wadhams, *Ice in the Ocean*. Amsterdam, The Netherlands: Gordon and Breach, 2000, pp. 140–166.

[34] D. J. Cavalieri, T. Markus, D. K. Hall, A. Ivanoff, and E. Glick, "Assessment of AMSR-E Antarctic winter sea-ice concentrations using aqua MODIS," *IEEE Trans. Geosci. Remote Sens.*, vol. 48, no. 9, pp. 3331–3339, Sep. 2010.

Sinéad Louise Farrell received the M.Sci. degree in Earth and space science and the Ph.D. degree from University College London, the University of London, London, U.K., in 2002 and 2007.

She joined the National Oceanic and Atmospheric Administration (NOAA) Satellite Oceanography and Climatology Division's Laboratory for Satellite Altimetry, Silver Spring, MD, as a National Research Council Research Associate in 2007. She is currently an Assistant Research Scientist at the Earth System Science Interdisciplinary Center, University of Maryland, College Park. She is a Visiting Scientist with both NOAA and the Cryospheric Sciences Branch at the NASA Goddard Space Flight Center. Her research interests lie in remote sensing of the Earth's polar regions to study cryospheric and oceanic processes.

Dr. Farrell is a member of the American Geophysical Union.

Nathan Kurtz received the B.S. degree in physics from Iowa State University, Ames, in 2004, and the M.S. degree in atmospheric physics and the Ph.D. degree from the University of Maryland Baltimore County (UMBC), Baltimore, in 2007 and 2009.

He is currently with the GESTAR Program, Morgan State University, Baltimore, MD. Prior to this he was with the NASA–UMBC Joint Center for Earth Systems Technology as a Research Associate in the Hydrospheric and Biospheric Research Group in 2010. His current research interests include microwave and laser remote sensing of sea ice and snow.

Dr. Kurtz is a member of the American Geophysical Union.

Laurence N. Connor received the B.S. degree in physics from Clemson University, Clemson, SC, in 1986, and the Ph.D. degree in electrical and computer engineering from the University of Colorado at Boulder, Boulder, in 1995.

He was a Postdoctoral Fellow with the Woods Hole Oceanographic Institution before joining the National Oceanic and Atmospheric Administration (NOAA) Office of Research and Applications, Silver Spring, MD. He is currently a Physical Scientist at the NOAA Satellite Oceanography and Climatology Division's Laboratory for Satellite Altimetry. He specializes in microwave scatterometry, radiometry, and altimetry techniques to study atmospheric, oceanic, and cryospheric processes.

Bruce C. Elder received the B.S. degree in geology from the University of New Hampshire, Durham, in 1990.

He began working at the U.S. Army Corps of Engineers Cold Regions Research and Engineering Laboratory, Hanover, NH, in 1985. His research interests lie in the study of sea ice dynamics and polar processes.

Carlton Leuschen (S'98–M'01) received the B.S. and Ph.D. degrees from the University of Kansas, Lawrence, in 1995 and 2001.

He is currently an Assistant Professor in electrical engineering and computer science at the University of Kansas. His interests include radar altimetry, radar sounding, and ground-penetrating radar.

Thorsten Markus (M'05) received the M.S. and Ph.D. degrees in physics from the University of Bremen, Bremen, Germany, in 1992 and 1995, respectively.

He was a National Research Council Resident Research Associate with the NASA Goddard Space Flight Center (GSFC) from 1995 to 1996 before joining the NASA–University of Maryland Baltimore County Joint Center for Earth Systems Technology, Baltimore, where he worked until 2002. He is currently the Head of the Cryospheric Sciences Branch in the Hydrospheric and Biospheric Sciences Laboratory, NASA GSFC, Greenbelt, MD. His research interests include satellite remote sensing and the utilization of satellite data to study cryospheric, oceanic, and atmospheric processes.

Dr. Markus is member of the American Geophysical Union.

David C. McAdoo received the Ph.D. degree from Cornell University, Ithaca, NY, in 1976.

He has been a Geophysicist with the National Aeronautics and Space Administration and, since 1984, with the National Oceanic and Atmospheric Administration (NOAA), Silver Spring, MD. He was Chief of the NOAA Geodynamics Branch from 1990 to 2000. He is currently a Research Geophysicist, at the NOAA Satellite Oceanography and Climatology Division's Laboratory for Satellite Altimetry, Silver Spring, MD. His recent research interests focus on polar geodynamics including derivation of marine gravity from satellite altimetry over ice-covered polar seas.

Dr. McAdoo is a member of the American Geophysical Union.

Ben Panzer received the B.S. and M.S. degrees in electrical engineering from the University of Kansas, Lawrence, in 2004 and 2007, respectively, where he is currently working toward the Ph.D. degree in electrical engineering.

His research is focused on ultrawideband radar hardware development and signal processing.

Jacqueline Richter-Menge received the B.S. degree in civil engineering and the M.C.E. degree from the University of Delaware, Newark, in 1979 and 1981, respectively.

She joined the U.S. Army Corps of Engineers Cold Regions Research and Engineering Laboratory (CRREL), Hanover, NH, as a Research Civil Engineer in the Snow and Ice Branch, in 1981. She served as Chief of the Snow and Ice Branch at CRREL from 1997 to 2006. Her research interests lie in the physical and mechanical properties of Arctic sea ice and understanding changes in the mass balance of the Arctic ice cover. She currently serves as Chair of the Scientific Ice Expeditions Science Advisory Committee. She has gained significant first-hand Arctic experience leading or participating in more than 15 field programs.

John G. Sonntag received the B.S. degree in aerospace engineering from Texas A&M University, College Station, in 1991 and the M.S. degree in aerospace engineering from the University of Texas, Austin, in 1993.

Since 1993, he has been with URS Corporation, working at the NASA Goddard Space Flight Center where he is the Instrument Team Lead for Operation IceBridge and a Senior Scientist with the Airborne Topographic Mapper project team. He specializes in the application of precise global positioning system positioning technology to airborne remote sensing problems and in the applications of airborne lidar mapping to polar science.